Journal of Intelligent Material Systems and Structures

Original Article

Journal of Intelligent Material Systems and Structures
2019, Vol. 30(3) 479–494

DOI: 10.1177/1045389X18812702
journals.sagepub.com/home/jim
SAGE

Shape memory alloy–actuated prestressed composites with application to morphing automotive fender skirts

Venkata Siva C Chillara[1], Leon M Headings[1], Ryohei Tsuruta[2], Eiji Itakura[3], Umesh Gandhi[2] and Marcelo J Dapino[1]

Abstract

This work presents smart laminated composites that enable morphing vehicle structures. Morphing panels can be effective for drag reduction, for example, adaptive fender skirts. Mechanical prestress provides tailored curvature in composites without the drawbacks of thermally induced residual stress. When driven by smart materials such as shape memory alloys, mechanically-prestressed composites can serve as building blocks for morphing structures. An analytical energy-based model is presented to calculate the curved shape of a composite as a function of force applied by an embedded actuator. Shape transition is modeled by providing the actuation force as an input to a one-dimensional thermomechanical constitutive model of a shape memory alloy wire. A design procedure, based on the analytical model, is presented for morphing fender skirts comprising radially configured smart composite elements. A half-scale fender skirt for a compact passenger car is designed, fabricated, and tested. The demonstrator has a domed unactuated shape and morphs to a flat shape when actuated using shape memory alloys. Rapid actuation is demonstrated by coupling shape memory alloys with integrated quick-release latches; the latches reduce actuation time by 95%. The demonstrator is 62% lighter than an equivalent dome-shaped steel fender skirt.

Keywords

shape memory alloy, prestressed, laminated composite, automotive, morphing, fender skirt, drag reduction, analytical model

Background on morphing structures

Morphing structures, defined as body panels that are capable of a gradual autonomous shape transformation, have gained importance in the automotive industry since they address the need to adapt a vehicle's shape for optimal performance over a range of operating conditions. Aerodynamic performance is critical at high speeds whereas other factors such as aesthetics, maneuverability, and ground clearance are a priority at low speeds. Requirements such as low weight, compactness, and system-level compatibility can be satisfied using adaptive laminated composites.

Automotive applications

A reduction of the coefficient of drag (C_D), defined as the force that resists vehicle motion in air, leads to improved fuel economy due to reduced engine load. The National Highway Traffic Safety Administration (NHTSA) mandates an improvement in fuel economy of 13 mpg[1] between 2015 and 2025 across all passenger vehicle segments (H-D Systems, 2013). Aerodynamic improvements can play a significant role toward meeting this mandate, since a 10% reduction in C_D can lead to a 2% increase in fuel economy. The factors contributing to aerodynamic drag in a passenger car are illustrated in Figure 1(a). Several geometric modifications to the vehicle body have been proposed for drag reduction (Hucho, 1987). Implementing geometric changes

[1]NSF IUCRC on Smart Vehicle Concepts, Department of Mechanical and Aerospace Engineering, The Ohio State University, Columbus, OH, USA
[2]Toyota Research Institute North America, Ann Arbor, MI, USA
[3]Toyota Motor Corporation, Susono, Japan

Corresponding author:
Venkata Siva C Chillara, NSF IUCRC on Smart Vehicle Concepts, Department of Mechanical and Aerospace Engineering, The Ohio State University, Columbus, OH 43210, USA.
Email: chillara.1@osu.edu

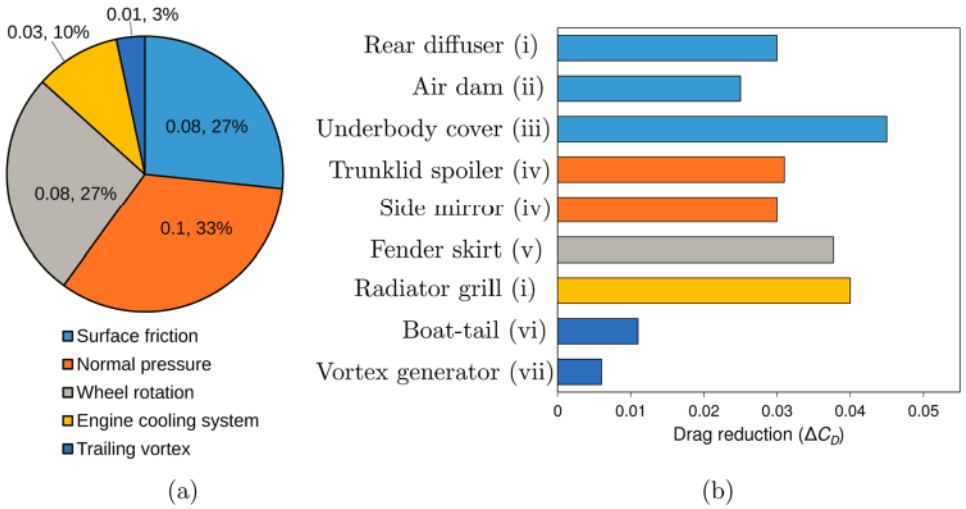

Figure 1. (a) Estimated contributions to the drag coefficient of a passenger car (data from Barnard (1996)) and (b) potential for drag reduction through the use of morphing structures. The color code used for morphing solutions in (b) correlates to the corresponding source of aerodynamic drag in (a). Sources for (b): (i) Hucho and Ahmed (1998), (ii) Costelli (1984), (iii) Buchheim et al. (1983), (iv) Hucho (1987), (v) Sunny (2011), (vi) Barnard (1996), and (vii) Koike et al. (2004).

as a rigid feature in the body is not always practical due to potential adverse effects on vehicle dynamics, aesthetics, and regulatory compliance. Morphing structures enable multifunctionality in body panels with an added possibility for weight reduction[2] and improved aesthetics. Active-geometry solutions that have a significant impact on aerodynamic performance are summarized in Figure 1(b). A fender skirt for a steered wheel is demonstrated in this article since it provides high drag reduction and is of practical interest.

For design purposes, a fender skirt is defined as an extension of a fender that covers the wheel, as shown in Figure 2(a). A fender skirt eliminates the turbulence caused by mixing of the flow stream originating from wheel rotation with the boundary layer of flow on the vehicle body (Sunny, 2011). Flat fender skirts that cover rear wheels have been implemented; examples include Ford Probe (prototypes I–V, 1979–84), Honda Insight (2000), and Volkswagen XL1 (2011). For steered wheels, however, dome-shaped skirts are required to avoid collision during wheel steer. The addition of a rigid dome-shaped skirt leads to increased vehicle width that could have adverse affects on aerodynamic performance and driving dynamics. These limitations can be addressed using adaptive fender skirts that are flat at high speed for optimal aerodynamic efficiency and switch to a domed shape to accommodate steering of the wheel at low speed (Figure 2). Under normal operating conditions, steering angles are typically less than 5° at highway speeds (>60 mile/h or 96.5 km/h), whereas large steering angles are common for low-speed operations such as parking maneuvers. The BMW Vision "Next 100 Years" (2016) is an example of a vehicle concept that features morphing fenders. In the BMW concept, the fender is the morphing element whereas the fender skirt is rigid.

Active laminated composites

Laminated composites with controllable curvature can serve as morphing elements in a dome-shaped structure such as a fender skirt. Embedded actuation is a preferred approach for smart composites as it enables compact and light-weight design. Bilgen et al. (2010) demonstrated a composite-based airfoil that can change camber (curvature) through the activation of piezoelectric macro-fiber composite laminae. However, piezoelectric actuators are ineffective for large bending due to their low strain of 0.1% (Kim et al., 2010). Inflatable laminae, driven by hydraulic or pneumatic power sources, can create flexure when used in conjunction with constrained layers (Chillara et al., 2016; Deimel and Brock, 2013; Philen et al., 2007); materials that are flexible but have high in-plane stiffness qualify as constraining layers. Implementation of inflatable structures is viable when they are paired with compact power sources such as smart material-driven electrohydraulic pumps (Chapman et al., 2005). Lacasse et al. (2014) developed fiber-reinforced polymeric composites with embedded shape memory alloy (SMA) wires. Upon activation, the SMA wires shrink in length to create flexure of the composite. SMA actuators have a high power-to-weight ratio and their high recoverable strain (up to 6%) enables large curvature (Huber et al., 1997). Due to their low weight and compactness, SMAs are candidates for automotive applications (Jani et al.,

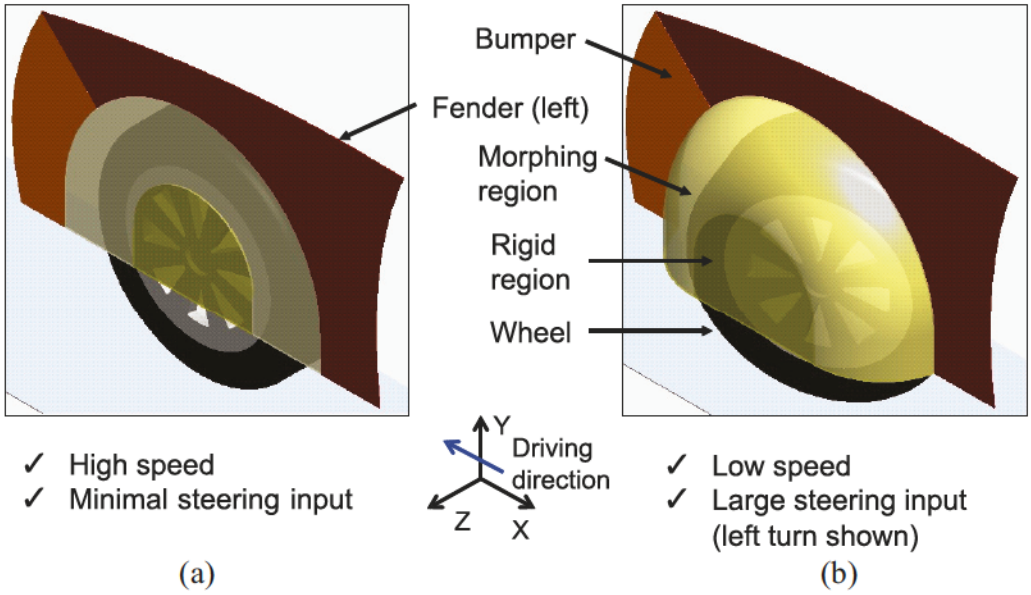

Figure 2. (a) Retracted flat shape and (b) deployed domed shape of a morphing fender skirt (shown in yellow).

2014). The Chevrolet Corvette (2014), for example, features a hatch vent that is opened using an SMA wire actuator, to release air trapped during the process of closing the trunk lid (General Motors, 2013).

Curvature in a composite can also be created using passive means such as residual stress (Hyer, 1981). Smooth curvature, devoid of kinks and cracks, is possible through the application of residual stress such that the input energy that is responsible for deformation is uniformly distributed across the domain. In fiber-reinforced polymeric composites, residual stress is imparted to the matrix through high-temperature curing (Daynes and Weaver, 2010; Hyer, 1981; Mattioni et al., 2008). Designs based on thermally induced stress are limited in function since the stress states of different laminae cannot be independently controlled. Furthermore, morphing based on thermally-prestressed composites involves multistability, a feature that may not be suitable for certain applications. On the other hand, mechanically-prestressed composites can exhibit single as well as multiple stable shapes (Chillara and Dapino, 2017b; Chillara et al., 2016). In these composites, residual stress can be generated in specific laminae by laminating them in a stretched condition. Mechanically-prestressed laminae act as internal springs in the composite since the applied prestress is irreversible. These springs can be paired with smart laminae that are required to actuate only in one direction. Chillara and Dapino (2017a, 2018) presented an SMA-actuated bistable composite in which the actuator is reset to its initial condition using mechanical prestress.

This study's main contribution is the development of composites with a generic planform whose curvature is controlled by SMA actuators acting against mechanical prestress; in contrast, past studies on prestressed composites are based on a rectangular geometry with passive laminae. Inspired by the literature on morphing aircraft, a model-based design procedure is presented for the implementation of smart composites in morphing automotive structures such as a fender skirt. The mechanics and kinematics of a particular fender skirt are discussed in section "Morphing structure configuration" to motivate composite design. An analytical model for a smart laminated composite is presented in section "Analytical model of an active composite rib." A design procedure for a composite element with trapezoidal planform is described in section "Design procedure for a composite rib." In section "Case study: fender skirt," a case study of a morphing fender skirt is presented to demonstrate the implementation of smart composites.

Morphing structure configuration

The configuration of an adaptive fender skirt is presented in this section to motivate the design of a morphing structure based on smart laminated composites. The types of laminae in a smart composite and their functions are also described.

Fender skirt

A fender skirt is envisioned as a dome-shaped structure that comprises identical curved composite ribs in a radial configuration (Figure 3(a)). A curved rib is created by laminating a mechanically-prestressed layer to a flexible panel. The central portion of the dome is rigid and flat in order to limit vehicle width, provide

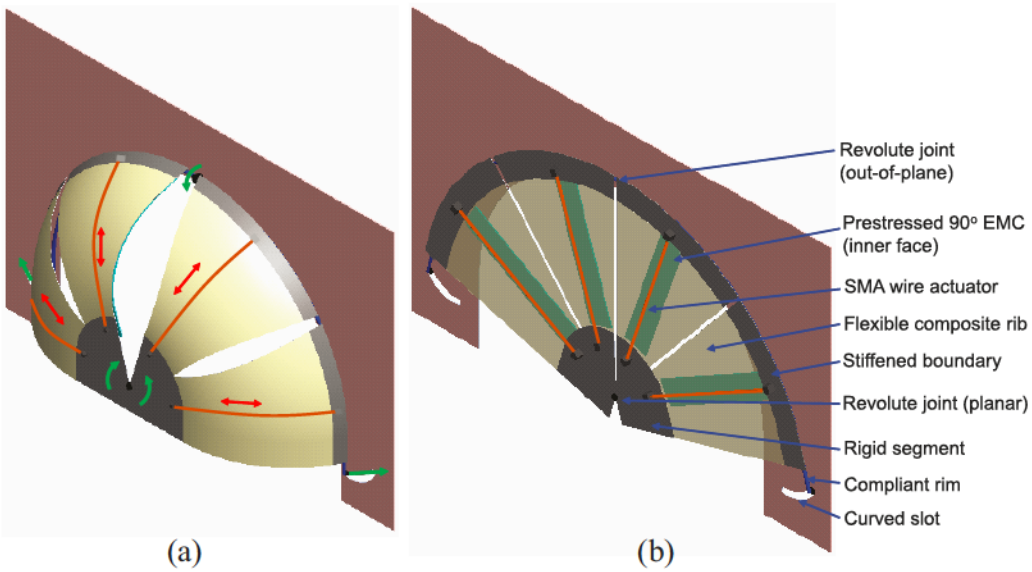

Figure 3. (a) Unactuated dome and (b) actuated flat shapes of a morphing fender skirt. The flexible segment in (b) is shown with transparency to highlight the details on the inner face; the skin is not shown.

structural integrity, and couple the ribs for a smooth global shape transition. The outer edges of the ribs are linked using a semicircular compliant rim. The ribs have a trapezoidal planform with SMA wires on their axis of symmetry.

An SMA wire is installed on a curved rib in the detwinned martensite phase at an offset from the geometric mid-plane; the actuator and the prestressed layer are placed on opposite faces of the rib to achieve antagonistic behavior. When heated, the wire transforms to austenite and thereby contracts to flatten the rib. Upon cooling, the SMA wire returns to the detwinned martensite phase due to the intrinsic prestress; the curved shape of the rib is recovered (Figure 3).

The mid-point of the rim is fixed whereas the rim ends slide in curvilinear slots in the fender. The reaction forces due to the flattening of each rib push the central hinge downward and the movable rim ends outward to reach the end of the curvilinear slots. Morphing between domed and flat shapes is such that the total surface area is constant. To relieve the resulting shear stress, a one-dimensional (1D) hinge (revolute joint) is included at the geometric center of the rib sectors. Each rib has a cylindrical curvature along the radial line of the fender skirt.

Assuming that the radially configured ribs are identical, one can model a single rib to design the global shape of the structure. The benefit of considering a single rib is that one can develop an analytical model that is computationally inexpensive when compared to a finite-element model of the entire structure. An analytical model of a rib guides planform design, material selection, and actuator design. The design considerations for the structure are discussed in detail in section "Design procedure for a composite rib."

Design considerations

For a compact passenger car with standard features, the maximum out-of-plane displacement of the wheel from the plane of the fender is measured to be 114.3 mm. The geometry of a steered wheel relative to its fender is shown in Appendix 1. To accommodate wheel rotation with a factor of safety of 1.33, the target out-of-plane displacement for the fender skirt is set to 152.4 mm. Pressure on the inner and outer faces of a fender skirt is a result of aerodynamic loads and cross-winds (lateral to vehicle motion), respectively. The maximum pressure at 144 km/h (90 miles/h) is estimated as 500 and 1000 Pa in the flat and domed shapes, respectively. The maximum allowable deflection of the structure in any shape is 5%. The mass of the morphing structure should be less than that of a typical 0.8-mm-thick steel automotive body panel. The ratio of the radius of the rigid segment to that of the fender is determined through an interference study in Solidworks (Dassault Systems). To prove the concept, modeling and demonstration of the fender skirt are shown at half-scale.

Laminated composite

The passive composite comprises constraining and prestressed laminae with an optional sandwiched core (Figure 4). A constraining layer is flexible but has high in-plane modulus relative to the prestressed layer. Candidate materials for the constraining layer include metals, plastics, and anisotropic fiber-reinforced composites. The constraining layer's shape is tailored to match the shape of an element or the entirety of a

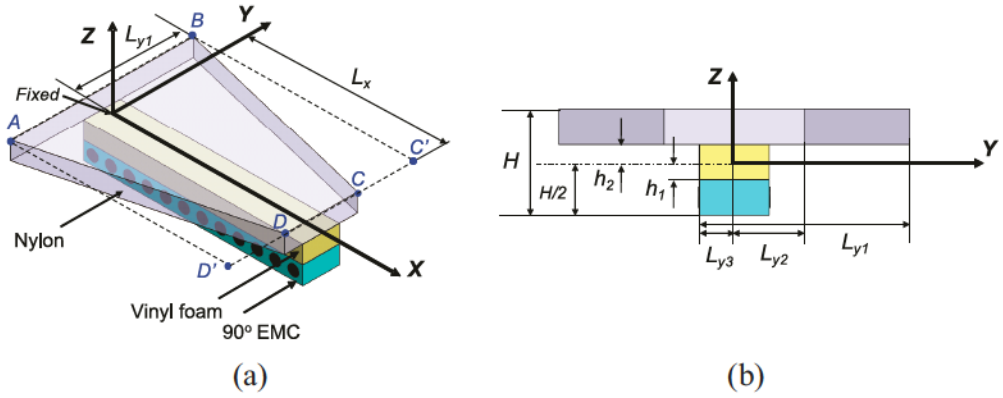

Figure 4. Schematic representation of a prestressed composite rib with a linearly varying tapered planform in the (a) isometric view and (b) *YZ* plane. Figure is not drawn to scale.

morphing structure. The prestressed layer is typically a stretchable elastic material, preferrably with zero in-plane Poisson's ratio; examples include elastomeric matrix composites (EMC) with 90° fibers (Murray et al., 2010). The benefit of restricting Poisson's ratio to zero is that the magnitude and orientation of a given cylindrical curvature of the composite's shape can be tailored using the magnitude and orientation of the applied prestress (Chillara and Dapino, 2017b).

In this work, the constraining layer is made of nylon plastic and the prestressed layer is a 90° EMC that is made of silicone rubber reinforced with unidirectional carbon fibers. The prestressed layer is laminated in a rectangular shape to ensure uniform distribution of prestress; it can be trimmed post lamination to match the composite's shape. A sandwiched core is included to increase the offset between the prestressed and constraining laminae, thus lowering the prestrain required to achieve a given curvature (discussed in section "Case study: fender skirt"). The core is a flexible material with a modulus that lies between that of the constraining and prestressed layers but is closer to that of the prestressed layer. Low-density vinyl foam is used as a sandwiched core over the area spanned by the prestressed layer.

Analytical model of an active composite rib

A composite rib is modeled based on classical laminate theory along with von Karman's hypothesis for small in-plane strains and moderate rotations. The composite's strain energy is formulated using displacement functions. Work done by actuation forces is computed using the variational principle. Minimization of the net energy using a Rayleigh–Ritz technique yields the displacement functions that define the shape of the composite. The strain formulation considered in this work

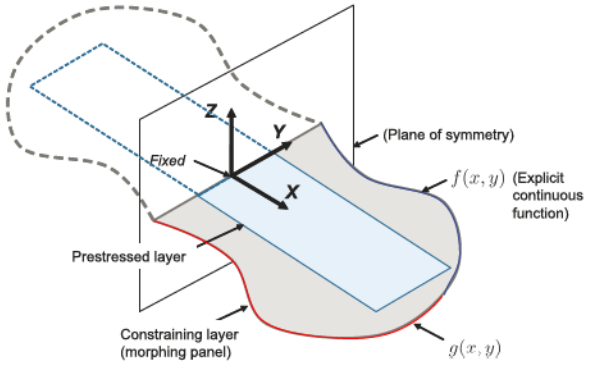

Figure 5. Schematic representation of a prestressed composite with an arbitrary planform shape that can be described using explicit continuous functions.

is based on the analytical modeling of fiber-reinforced polymeric laminates proposed by Hyer (1982).

The modeling approach presented in this section is applicable to composites where the constraining layer has arbitrary planform shapes that can be defined using explicit continuous functions (Figure 5). Examples of explicit functions include $h(x,y) = k_1x + k_2y$ and $h(x,y) = k_3x^2 + k_4xy + k_5y^2$ for linear and elliptical planform shapes, respectively. Strain energy can be calculated by integrating the continuous functions over the composite's volume. For smooth complex shapes defined using multiple shape functions, displacements would have to be modeled using high-order polynomials. Symmetry in composite shape, if present, can be considered to simplify the displacement polynomials prior to computation. It is assumed that prestrain is uniform throughout the prestressed layer. Thus, the prestressed layer is modeled as a rectangle.[3] The modeling approach is demonstrated for a trapezoidal composite rib with linearly varying planform (as in Figure 4).

Strain energy computation

The geometry of a composite rib is shown in Figure 4. The rib is clamped at the origin and is symmetric about the XZ plane; all points in the composite, except the origin, are unconstrained. The composite comprises a trapezoidal panel bonded to a rectangular 90° EMC strip. A sandwiched core is included to provide sufficient curvature at low prestrain (discussed in section "Design procedure for a composite rib"); the areal dimensions of the core are the same as those of the EMC. The taper in a trapezoidal panel is defined as

$$\omega = \frac{L_{y1} - L_{y2}}{L_x} \tag{1}$$

The minimum value of ω is zero, whereas the maximum value corresponds to $L_{y2} = 0$ and is equal to the aspect ratio L_{y1}/L_x.

The strain energy of the tapered panel $ABCD$, obtained by subtracting the energy in the triangular regions ADD' and BCC' from the energy in the rectangle $ABC'D'$ (Figure 4), is written as

$$\Phi_p = \left(\int_0^{L_x}\int_{-L_{y1}}^{L_{y1}} d\Phi_p dy dx\right) - \left(\int_0^{L_x}\int_{L_{y1}-\omega x}^{L_{y1}} d\Phi_p dy dx\right) - \left(\int_0^{L_x}\int_{-L_{y1}}^{\omega x - L_{y1}} d\Phi_p dy dx\right) \tag{2}$$

The integrand in equation (2) is defined as

$$d\Phi_p = \int_{h_2}^{H/2}\left(\frac{1}{2}Q_{11}^{(p)}\varepsilon_x^2 + Q_{12}^{(p)}\varepsilon_x\varepsilon_y + \frac{1}{2}Q_{22}^{(p)}\varepsilon_y^2 + \frac{1}{2}Q_{16}^{(p)}\gamma_{xy}\varepsilon_x + \frac{1}{2}Q_{26}^{(p)}\gamma_{xy}\varepsilon_y + \frac{1}{2}Q_{66}^{(p)}\gamma_{xy}^2\right)dz \tag{3}$$

where $Q_{ij}, \{i,j = 1,2,6\}$ are the plane stress-reduced stiffnesses (Reddy, 1997) and ε_x, ε_y, and γ_{xy} are the strains in the composite (Chillara and Dapino, 2017b).

The respective strain energies of the core and 90° EMC are

$$\Phi_c = \int_0^{L_x}\int_{-L_{y3}}^{L_{y3}}\int_{-h_1}^{h_2}\left(\frac{1}{2}Q_{11}^{(c)}\varepsilon_x^2 + Q_{12}^{(c)}\varepsilon_x\varepsilon_y + \frac{1}{2}Q_{22}^{(c)}\varepsilon_y^2 + \frac{1}{2}Q_{16}^{(c)}\gamma_{xy}\varepsilon_x + \frac{1}{2}Q_{26}^{(c)}\gamma_{xy}\varepsilon_y + \frac{1}{2}Q_{66}^{(c)}\gamma_{xy}^2\right)dz dy dx \tag{4}$$

Table 1. Polynomial coefficients corresponding to a nonlinear stress function for a 90° EMC made of carbon fiber–reinforced silicone, obtained from a uniaxial tensile test (Chillara et al., 2016).

p_1	p_2	p_3	p_4
-0.698×10^6	2.29×10^6	-2.306×10^6	1.598×10^6

$$\Phi_{90} = \int_0^{L_x}\int_{-L_{y3}}^{L_{y3}}\int_{-H/2}^{-h_1}\left(\frac{p_1}{5}(\varepsilon_{90} - \varepsilon_x)^5 + \frac{p_2}{4}(\varepsilon_{90} - \varepsilon_x)^4 + \frac{p_3}{3}(\varepsilon_{90} - \varepsilon_x)^3 + \frac{p_4}{2}(\varepsilon_{90} - \varepsilon_x)^2 + \frac{1}{2}Q_{22}^{(90)}\varepsilon_y^2 + \frac{1}{2}Q_{66}^{(90)}\gamma_{xy}^2\right)dz dy dx \tag{5}$$

The coefficients p_1 through p_4 are those of a quartic polynomial that describes the nonlinear stress function of a 90° EMC (Chillara et al., 2016). These coefficients, shown in Table 1, are determined experimentally from a uniaxial tensile test. The total strain energy of the system is expressed in terms of the strain energies of the constituent layers as

$$\Phi = \Phi_p + \Phi_c + \Phi_{90} \tag{6}$$

Work done by an external force

Chillara and Dapino (2017a) presented an analytical approach to model in-plane SMA wire actuators using a pair of tangential point forces. Using this approach, in-plane actuation is modeled in the configuration shown in Figure 6(a).

The actuation force is expressed in terms of its position vector ($\vec{r}$) as

$$\vec{F} = -F\frac{\partial\vec{r}}{\partial x}\Big/\left|\frac{\partial\vec{r}}{\partial x}\right| \tag{7}$$

where $\vec{r}$ is written in terms of the position of the point ($\vec{r}_0$) on the mid-plane and the normal ($\vec{n}$) of magnitude m at $\vec{r}$

$$\vec{r} = \vec{r}_0 + m\vec{n} \tag{8}$$

$$\vec{r} = \vec{r}_0 + m\frac{\left(\frac{\partial\vec{r}_0}{\partial x} \times \frac{\partial\vec{r}_0}{\partial y}\right)}{\left|\frac{\partial\vec{r}_0}{\partial x} \times \frac{\partial\vec{r}_0}{\partial y}\right|}, \quad \text{where} \quad \vec{r}_0 = ((x + u_0)\boldsymbol{i} \quad + (y + v_0)\boldsymbol{j} + w_0\boldsymbol{k}) \tag{9}$$

and u_0, v_0, and w_0 are the displacements of an arbitrary point on the composite's mid-plane in the X, Y, and Z directions, respectively. Virtual work done by the actuation force is written as

$$\delta W_F = -\vec{F}\cdot\delta\vec{r}|_{\{L_x,0\}} \tag{10}$$

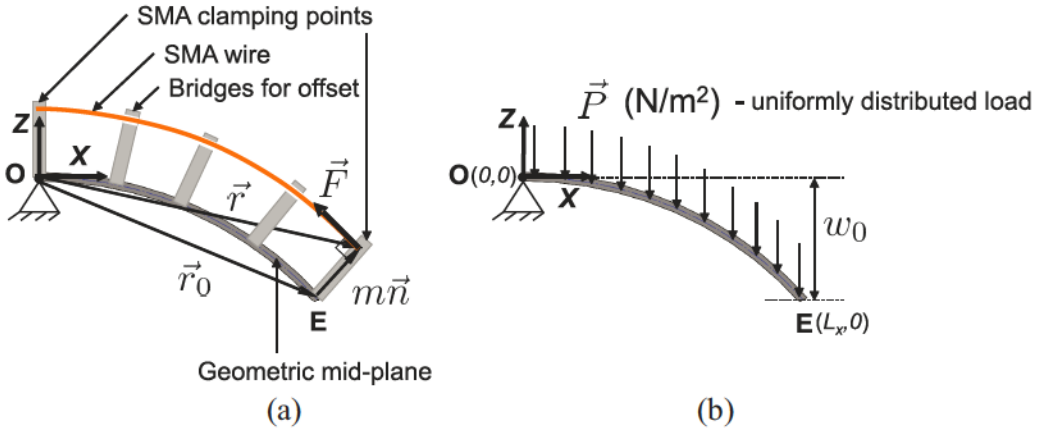

Figure 6. Configuration of (a) in-plane force ($\vec{F}$) and (b) uniformly distributed vertical force ($\vec{P}$) on a curved plate that represents the prestressed laminated composite rib. The SMA wire slides freely across the bridges. Note: The schematics are not drawn to scale; not all layers are shown.

For stiffness calculation, virtual work done by a uniformly distributed pressure of magnitude P (Figure 6(b)) can be expressed as

$$\delta W_P = \left(\int_0^{L_x}\int_{-L_{y1}}^{L_{y1}} Pw_0 \mathrm{d}y\mathrm{d}x\right) - \left(\int_0^{L_x}\int_{L_{y1}-\omega x}^{L_{y1}} Pw_0 \mathrm{d}y\mathrm{d}x\right) - \left(\int_0^{L_x}\int_{-L_{y1}}^{\omega x - L_{y1}} Pw_0 \mathrm{d}y\mathrm{d}x\right) \tag{11}$$

Composite displacements and shape computation

Displacements u_0, v_0, and w_0 are assumed to be polynomial functions with unknown coefficients. The composite is expected to have non-uniform curvature due to its trapezoidal planform. Therefore, w_0 is defined by a complete quartic polynomial in order to describe the variation in curvature. Since the curvature is expected to be about the Y axis, the polynomial order for u_0 is considered to be higher than that of v_0. Displacements u_0 and v_0 are assumed to have orders 5 and 3, respectively. Given that the composite is symmetric about the Y axis, v_0 is assumed to be odd in y and even in x. Although the composite lies in the $x>0$ space, u_0 can be approximated by assuming symmetry about the Y axis. This choice does not affect the solution since strain energy is computed only for $x>0$. Therefore, u_0 is odd in x and even in y. The out-of-plane displacement w_0 is even in x and y. The resulting displacement polynomials have 14 coefficients (c_i) in total. The equilibrium shapes of the composite are obtained as a function of the external forces by minimizing the net energy using the variational Rayleigh–Ritz approach

$$\sum_i \frac{\partial(\Phi - W_F - W_P)}{\partial c_i} = 0 \tag{12}$$

where i ranges from 1 to 14. The 14 nonlinear equations are solved for the coefficients using the Newton–Raphson method.

Actuation using SMA wire

An SMA undergoes a large recoverable strain as the material transforms from austenite to martensite when it is cooled below a certain temperature or mechanically stressed. The strain can be recovered by heating the material so that it transforms back into austenite. The constitutive behavior of a 1D SMA can be modeled using thermodynamic relations to obtain stress as a function of strain, temperature, and martensite volume fraction. A kinetic law describing the material's phase as a function of stress and temperature is used in conjunction with the constitutive law. The volume fraction of martensite is commonly described in empirical form as an exponential (Tanaka et al., 1986) or cosine function (Liang and Rogers, 1990) of temperature. Brinson (1993) developed a constitutive model for SMAs where the martensite volume fraction has temperature-induced and stress-induced components. Since the choice of the function used to describe volume fraction does not affect the model's accuracy (Brinson and Huang, 1996), the multivariant constitutive model, as formulated by Brinson, is employed to describe the composite's actuation.

Dano and Hyer (2003) presented analytical modeling and experiments to calculate the curved shapes of composites as a function of actuation forces applied by straight SMA tendons. Hufenbach et al. (2006) presented design strategies for bistable morphing composites using actuators in a laminar configuration.

Table 2. Geometric parameters that correspond to a single composite rib of a half-scaled fender skirt.

L_x	L_{y1}	L_{y2}	ω	L_{y3}	H	h_1	h_2
152.4	76.2	28.55	0.312	31.75	5.975	2.1875	−0.9875

All parameters are expressed in millimeters except for ω, which is unitless.

Simoneau et al. (2014) and Lacasse et al. (2014) developed a finite-element model to characterize curvature in fiber-reinforced composites that are actuated by embedded SMAs. They presented parametric studies on the effect of the composites' material properties on their shape and actuation requirements. In our model, an analytical approach is presented for composites with laminar SMA actuators that work against an intrinsic mechanically induced prestress in pre-curved composites.

The SMA wire is installed at an offset m from $\overline{OE}$ and is clamped above points O and E, as shown in Figure 6(a), to ensure that it does not induce twist in the composite. The wire is installed on a curved composite in the detwinned martensite phase. When heated so that the wire transforms to austenite, it contracts to flatten the composite. Upon deactivation, the SMA becomes detwinned due to prestress in the composite. For an SMA mounted at an offset m from the mid-plane, the expressions for actuator strain in terms of composite strain were derived by Chillara and Dapino (2017a). Based on those expressions, actuator strain (ε) is written in terms of the respective strains $\varepsilon_x^{(s)}$ and $\varepsilon_x^{(i)}$ in the unactuated and intermediate shapes, as

$$\varepsilon = \frac{(1+\varepsilon_x^{(i)})(1+\varepsilon_L)}{(1+\varepsilon_x^{(s)})} - 1 \tag{13}$$

where $\varepsilon_x^{(s)}$ and $\varepsilon_x^{(i)}$ are expressed in terms of mid-plane displacements (Chillara and Dapino, 2017b), and ε_L is the recoverable strain in the SMA. Per equations (12) and (13), strain can be calculated for a given actuation force.

Design procedure for a composite rib

Based on the model presented in section "Analytical model of an active composite rib," parametric studies are presented to analyze the effect of EMC prestrain, laminate thickness and stiffness, and SMA wire properties on the composite's shape. The design of composite ribs is explained for the half-scaled fender skirt discussed in section "Fender skirt." The geometric and material parameters of the ribs considered for fender skirt design are listed in Tables 2 and 3, respectively.

Table 3. Material properties and thicknesses of the laminae considered for modeling and fabrication.

	Nylon panel	Vinyl foam core	Prestressed 90° EMC
Thickness (mm)	0.8	3.125	2
E_1 (MPa)	1000	30	Nonlinear
E_2 (MPa)	1000	30	1.5
G_{12} (MPa)	500	15	0.4
$\nu_{12} = \nu_{21}$	0.28	0.33	0

EMC: elastomeric matrix composite.

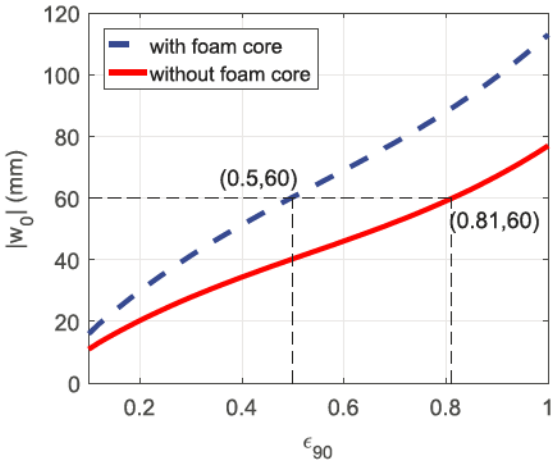

Figure 7. Influence of EMC prestrain ε_{90} on the out-of-plane displacement (w_0) at (L_x, 0) on the composite rib.

Passive composite

The design requirement for the out-of-plane displacement of a half-scale curved rib is 76.2 mm; out-of-plane displacement is defined as w_0 at $E(L_x, 0)$ as illustrated in Figure 6(b). Subtracting the offsets due to the hinges on the rib and mounts on the structure, the target w_0 is set to 60 mm. The EMC prestrain (ε_{90}) required to achieve the target w_0 is identified from the w_0 versus ε_{90} plot in Figure 7. The width and thickness of the EMC are chosen based on assembly constraints. It is seen that the inclusion of a vinyl foam core reduces prestrain requirements for a given out-of-plane deflection. For $w_0 = 60$ mm, ε_{90} is 26% lower in the presence of a foam layer. With the foam layer added, the required EMC prestrain in the rib is calculated to be 0.5. It is emphasized that the nonlinear dependence of w_0 on ε_{90} resembles the nonlinear material response of an EMC (see equation (5) and Table 1), as discussed by Chillara and Dapino (2017b).

Based on the calculated EMC prestrain ε_{90} of 0.5, the modulus (related to $Q_{ij}^{(p)}$) and thickness ($H/2 - h_2$) of the panel can be refined based on Figure 8. The simulated modulus range corresponds to plastics, such

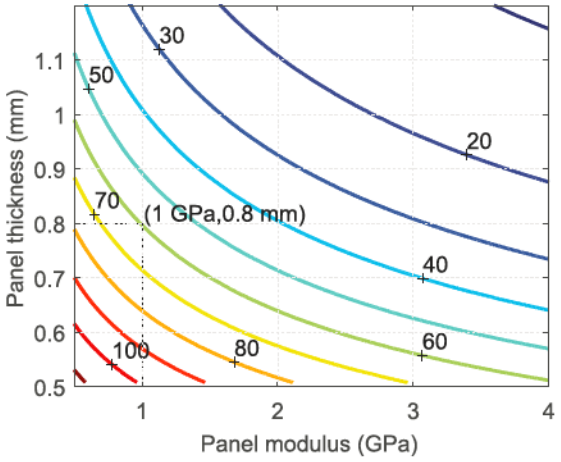

Figure 8. Effect of panel modulus and thickness on the out-of-plane displacement w_0, evaluated at $\varepsilon_{90} = 0.5$. Isometric lines correspond to w_0 in millimeters at $(L_x, 0)$.

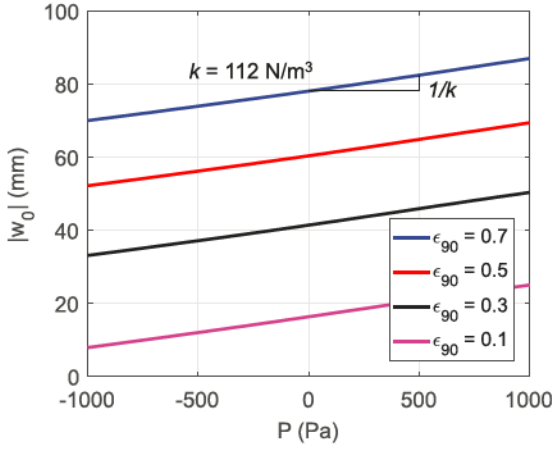

Figure 9. Out-of-plane displacement at $(L_x, 0)$ as a function of a vertical uniform pressure of magnitude P.

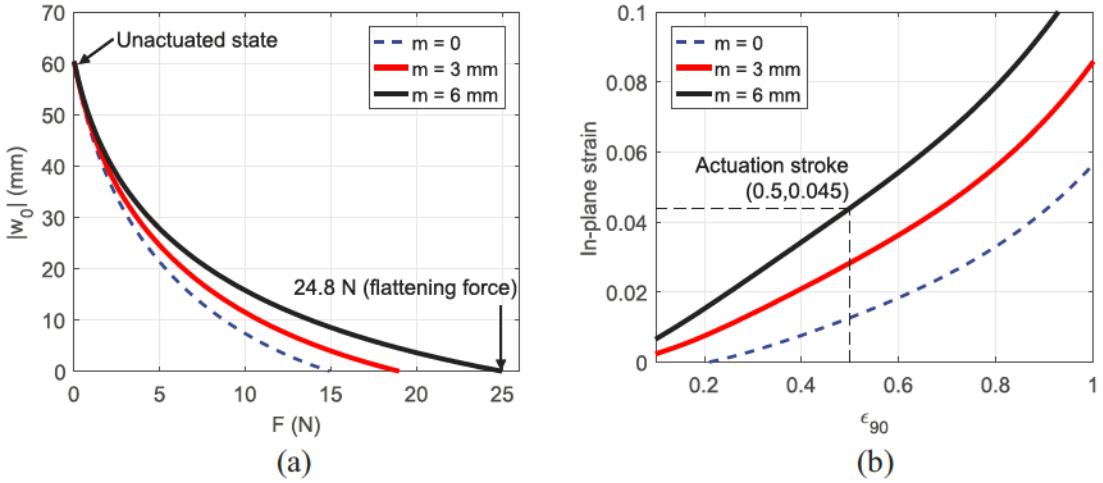

Figure 10. Plots to calculate the (a) force and (b) stroke required to flatten the composite.

as nylon, that allow the panel's edges to conform to the skin for a smooth external appearance. Other material options include commonly used automotive materials such as aluminum and steel. For demonstration purposes, it is assumed that the panel is made of nylon of modulus 1 GPa. For $w_0 = 60$ mm, the corresponding thickness is obtained from Figure 8 as 0.8 mm.

Figure 9 shows the out-of-plane deflection w_0 at $(L_x, 0)$ as a function of a uniformly distributed vertical pressure P. Stiffness, defined as the product of the slope of the pressure-deflection curve (k) and panel area, is calculated to be 1.78 N/mm. It is observed that stiffness is independent of EMC prestrain. Tip deflections at -500 and -1000 Pa are 2.7% and 5.4% of rib length, respectively. Therefore, for small deflections, stiffness is constant and independent of the shape of the passive composite. However, stiffness depends on the modulus and thickness of the laminae (simulation not shown). It is emphasized that the design for stiffness is based on an unconstrained edge at $x = L_x$ whereas in the fender skirt, the edges at $x = 0$ and $x = L_x$ are hinged and fixed, respectively. The added boundary conditions and the structure's kinematic design are expected to augment the designed stiffness. Simulation of the structure's stiffness requires a finite element analysis that is beyond the scope of this article.

SMA actuation

Figure 10(a) shows the deflection at $(L_x, 0)$ as a function of an in-plane actuation force F. The force that flattens the composite pertains to $w_0 = 0$. Flattening force increases with an increase in the offset m of force application from the mid-plane. Actuator stroke, calculated as the in-plane strain at $z = m$, also increases with an increase in m (Figure 10(b)). An offset of 6 mm is

Table 4. Material properties of a NiTi-6 shape memory alloy wire based on measurements from thermomechanical tensile tests and differential scanning calorimetry.

E_M (GPa)	E_A (GPa)	C_M (MPa/°C)	C_A (MPa/°C)	σ_s^{cr} (MPa)	σ_f^{cr} (MPa)
20	40	6.3	7.5	10	120
A_s (°C)	A_f (°C)	M_s (°C)	M_f (°C)	ε_L	
48	62	23	7	0.045	

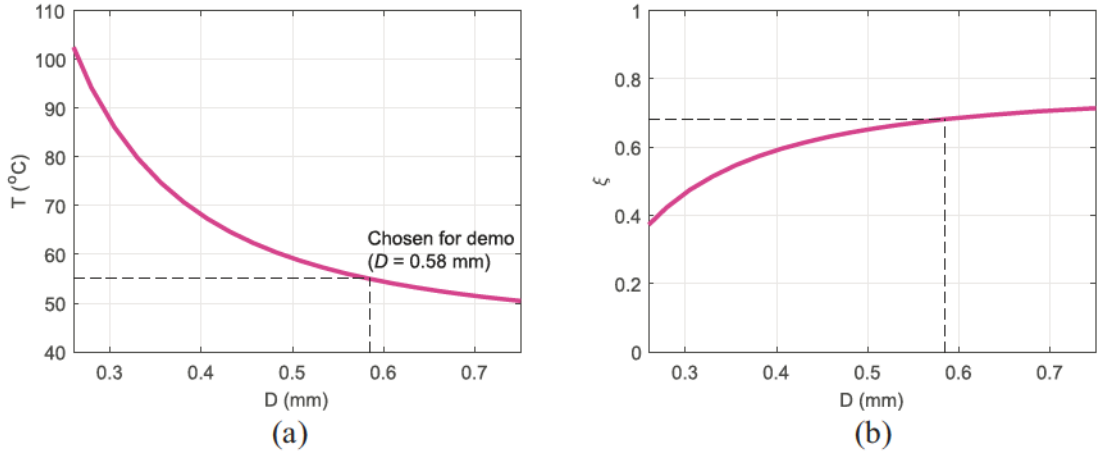

Figure 11. (a) Actuation temperature and (b) martensite volume fraction of an SMA wire post actuation, as a function of its diameter.

applied such that the actuator stroke matches a recoverable strain of 0.045 of the chosen NiTi #6 (Fort Wayne Metals Inc.) SMA wire. The flattening force at $m = 6$ mm is 24.8 N.

For an automotive application, the selection of an SMA material is influenced by the range of operating temperatures. The austenite start and finish temperatures should be higher than the maximum operating temperature, whereas the martensite start and finish temperatures should be lower than the minimum operating temperature. For demonstration purposes, a NiTi #6 SMA with properties listed in Table 4 is considered in the design. Heating temperatures required to generate a flattening force of 24.8 N are calculated for various values of NiTi #6 wire diameter (Figure 11(a)). The corresponding change in martensite volume fraction is plotted in Figure 11(b) per the following expression for transformation from martensite to austenite, when $((\pi D^2)/4)C_A(T - A_f) < F < ((\pi D^2)/4)C_A(T - A_s)$

$$\xi = \frac{\xi_0}{2}\left\{\cos\left(\frac{\pi}{A_s - A_f}(T - A_s - \frac{4F}{\pi D^2 C_A})\right) + 1\right\} \quad (14)$$

where C_A is the stress–temperature coefficient for the austenite phase, and A_s and A_f are the austenite start and finish temperatures, respectively. In martensite to austenite transformation, stress delays phase change, thereby requiring higher temperatures than in the stress-free case to achieve actuation. For a given flattening force, a higher wire diameter corresponds to lower stress and hence lower actuation temperature. As a consequence of the lowering of stress and actuation temperature, the change in martensite volume fraction reduces with an increase in wire diameter. An SMA wire of 0.58 mm diameter is chosen for demonstration; the wire is heated to 55°C to flatten the composite. Using the kinetic law for austenite to martensite transformation (Brinson, 1993), it can be verified that the volume fraction changes from $\xi = 0.68$ (from Figure 11(b)) to $\xi = 1$ when the composite returns to the domed shape after the actuation input is switched off.

Case study: fender skirt

Fabrication and validation of composite ribs

The steps involved in the fabrication of the fender skirt are illustrated in Figures 12 and 13. The ribs are cut out of a sector of a circular nylon panel with an included angle of 148° and a radius of 228.6 mm. To accommodate the rigid portion (Figure 3(b)), a smaller sector of radius 76.2 mm is removed from the larger sector prior to rib preparation (Figure 12(a)). An EMC strip is stretched to 1.5 times its stress-free length and held between a pair of grips (Figure 12(b)). The prestressed EMC is laminated with a sandwiched vinyl foam (Divinycell, 48 kg/m^3, Fiberglast Developments Corp.)

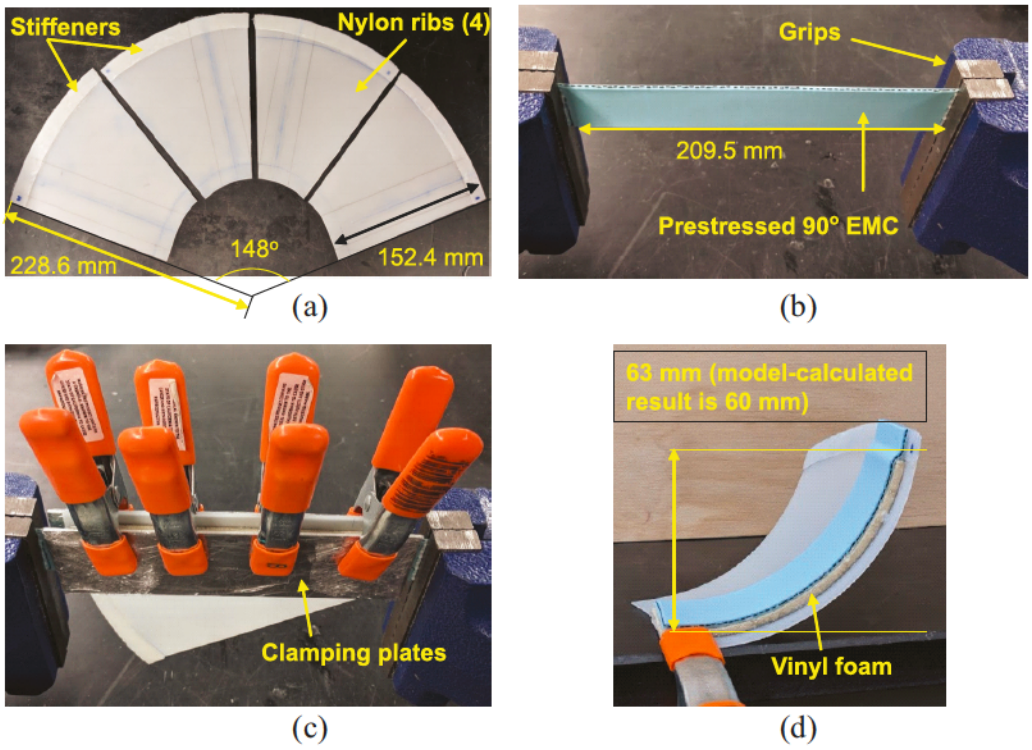

Figure 12. Fabrication procedure for a prestressed composite rib. (a) Ribs cut out of a sector of nylon sheet; (b) a 90° EMC stretched and held between a pair of grips; (c) lamination of the nylon panel, vinyl foam core, and EMC under pressure; and (d) final free shape of the prestressed rib.

core to each rib using a flexible adhesive (automarine silicone sealant by DAP products) as shown in Figure 12(c). Upon curing for 24 h, a cylindrically curved rib is obtained (Figure 12(d)). The out-of-plane displacement of the rib is measured to be 63 mm. The measured displacement agrees well with the model-calculated design value of $w_0 = 60$ mm.

The prestressed EMC is oriented asymmetrically relative to the trapezoidal nylon rib such that the in-plane reaction forces generated during actuation are aligned in the horizontal and vertical directions relative to the structure to enable flattening. As the fender skirt flattens, the vertical component of reaction force aids in rotation of the central hinge and the horizontal component forces the ends of the rim to slide outwards. Stiffeners are added to the rim-side edges of the ribs to prevent buckling at the hinges during morphing (Figure 12(a)); the effect of the stiffener on the out-of-plane displacement is negligible.

Fabrication of the fender skirt

The two halves of the central region are 3D-printed using nylon and are connected by the central hinge. The curved ribs are then riveted to the rigid segment to obtain a domed shape (Figure 13(a)). The hinges on the ribs are linked together using a compliant rim made of copper wire. NiTi #6 SMA wires of 0.58 mm diameter are trained using cyclic strain at a constant temperature of 80°C. The wires are then installed on 3-mm-thick polycarbonate bridges that are bonded to the outer face of the panel; bridges are added to maintain an offset of 6 mm from the mid-plane (Figure 13(b)). The wire is clamped on the outer end of the panel and is latched at the inner end. The response time of the actuator SMA, and hence the structure, is on the order of seconds. In order to quickly return from an intermediate shape to the domed shape in emergency maneuvers, a rotary latch is designed to release the actuator SMA (Figure 13(c)). Latch design details are presented in Appendix 2.

The rim is connected, at two points near its center, to a wooden frame that represents the fender (Figure 13(d)). The fender skirt is covered by a skin that extends smoothly onto the fender (Figure 13(e)). The skin is made of a polyether-polyurea copolymer, commonly known as Spandex. The skin material used is easily stretchable and slides smoothly on the fender skirt. There is no shear in the skin due to the rotation of the central revolute joint in the fender skirt.

Demonstration

The actuation sequence for the demonstrator is illustrated in Figure 14. The SMAs that actuate the composite and the latch are referred to as actuator SMA and latch SMA, respectively. In the unactuated state,

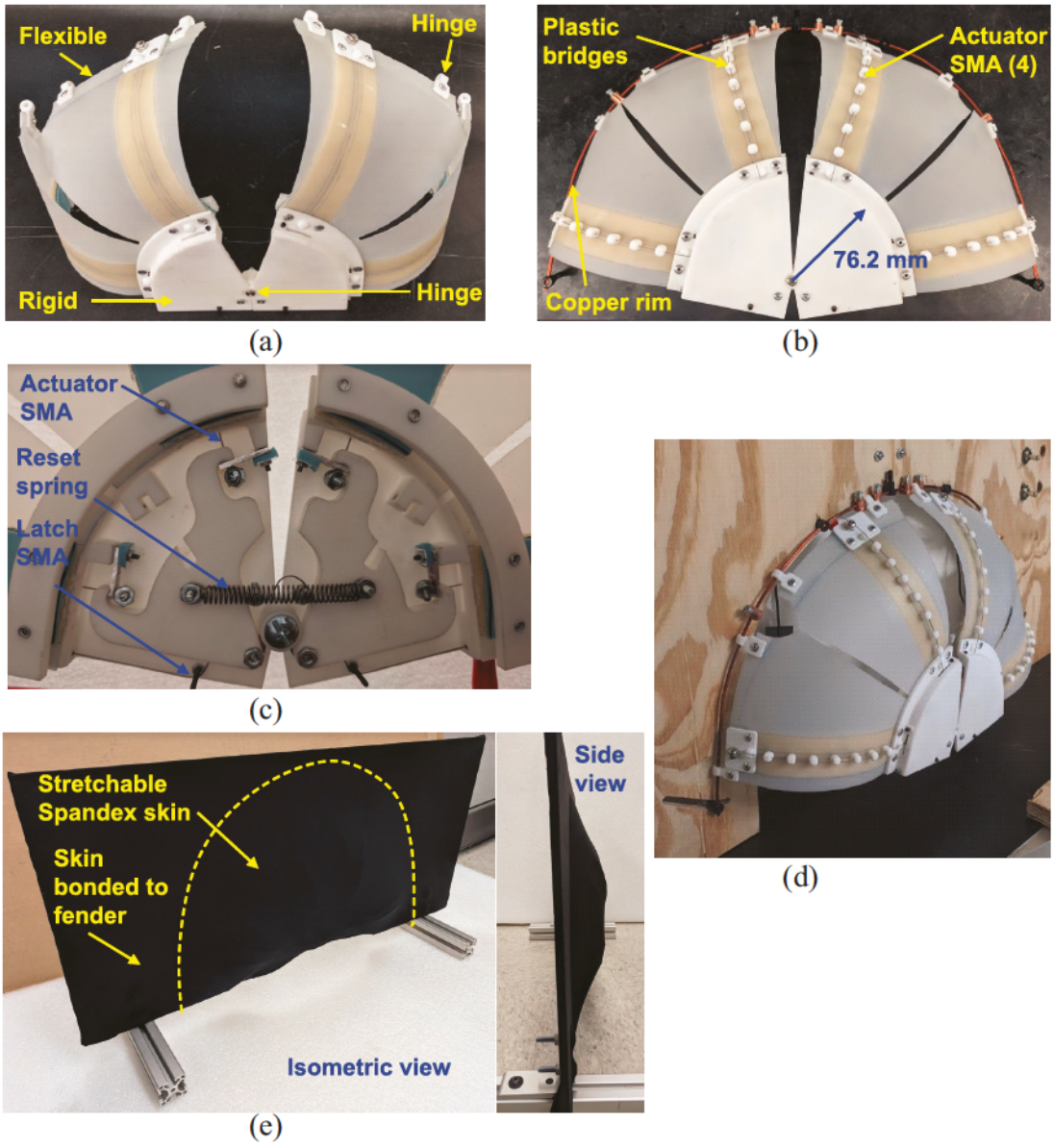

Figure 13. Fabrication procedure for a half-scale fender skirt demonstrator. (a) Assembly of the ribs and a 3D-printed rigid structure; (b) linkage of the outer ends of the ribs using a compliant copper rim; (c) elements of the latch mechanism on the back of the rigid structure; (d) fender skirt assembled on a wooden frame; and (e) stretchable Spandex skin installed on the fender skirt. The skin covers the morphing fender as well as the surrounding wooden frame representing the fender.

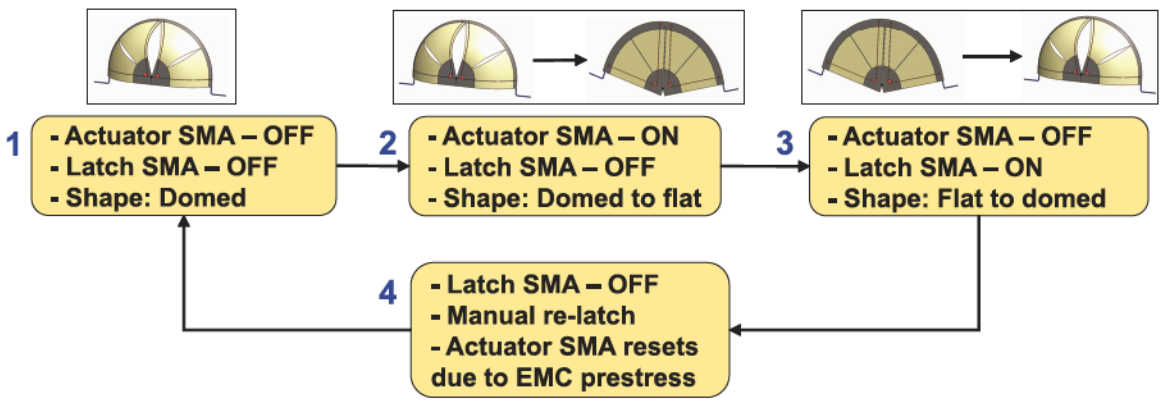

Figure 14. Actuation sequence for the demonstration of a morphing fender skirt.

Table 5. Summary of results from the fender skirt demonstrator.

Parameter	Value
Design value of w_0 in mm for half-scale demo	60 mm
EMC prestrain ε_{90} calculated for $w_0 = 60$ mm	0.5
Measured value of w_0 in physical composite rib	63 mm
Mass of the fender skirt demonstrator	355 g
Mass saving relative to a 0.8-mm-thick steel body panel	62%
Actuation current	4.6 A at 2.7 V
Actuation power	12.4 W (3.1 W per SMA)
Actuation time when SMAs are air-cooled	9.1 s (flattening), 10 s (recovery)
Actuation time when SMAs are unlatched	9.1 s (flattening), 0.5 s (recovery)

EMC: elastomeric matrix composite; SMA: shape memory alloy.

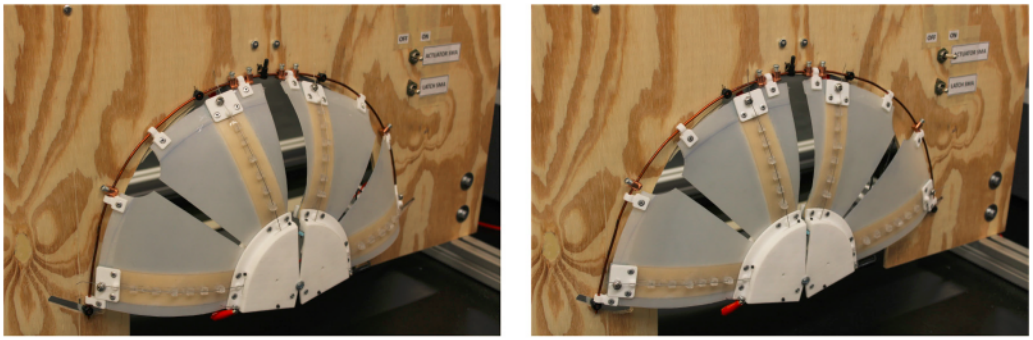

(a) (b)

Figure 15. (a) Unactuated domed shape and (b) actuated flat shape of a half-scale morphing fender skirt demonstrator.

the fender skirt is in the domed shape (stage 1). The structure is flattened by activating the actuator SMAs in the latched state (stage 2). From an intermediate shape, the structure is returned to the domed shape by activating the latch SMA (stage 3); the actuator SMA is turned off in this stage. In the final stage, the latch SMA is turned off and the actuator SMAs are manually latched back for subsequent actuation (Table 5).

The unactuated and actuated shapes of the fender skirt are shown in Figure 15. The actuator SMAs on each half of the structure are electrically connected in series. The electrical branches on either half are connected in parallel. The out-of-plane deformation of the fender skirt is measured using a motion capture system (Figure 16(a)). A reflective marker, bonded to the rigid segment, is tracked using a set of four cameras. The steps involved in shape measurement using a motion capture system are discussed in detail by Chillara and Dapino (2017b). The coordinates of the marker relative to those of a reference marker on the frame are obtained for one morphing cycle.

Figure 16(b) shows the out-of-plane displacement of a fender skirt that is flattened by heating the actuator SMAs and returned to the domed shape by: (1) cooling the SMAs in forced air (table fan), (2) unlatching the actuator SMAs from an intermediate shape, and (3) unlatching from a flat shape. In the domed shape, the out-of-plane displacement is measured to be 58.5 mm, which is within 10% of the free deflection of an individual rib (63 mm per Figure 12(d)). The measured fender skirt displacement is also within 3% of the design value of 60 mm used in the modeling of the individual ribs. Therefore, the domed shape validates the modeling of the passive composite. Flattening of the structure ($w_0 = 0$ mm) when heated and its return to the initial domed shape ($w_0 = 58.5$ mm) when cooled validates the model-based design of the actuator SMAs; heating and cooling are represented in Figure 16(b) by thin and thick black curves, respectively. With the use of latches, the extension time is reduced to the order of milliseconds, thereby making SMA-actuated composites applicable to conditions involving high-steering rate maneuvers.

Conclusion

The analytical model for active prestressed composites serves as a tool for shape tailoring, composite material selection, and actuator design. The model has been validated for the calculation of static shapes of the composite. Future developments may include an analytical thermomechanical dynamic model of the SMA-driven structure to calculate deployment speeds.

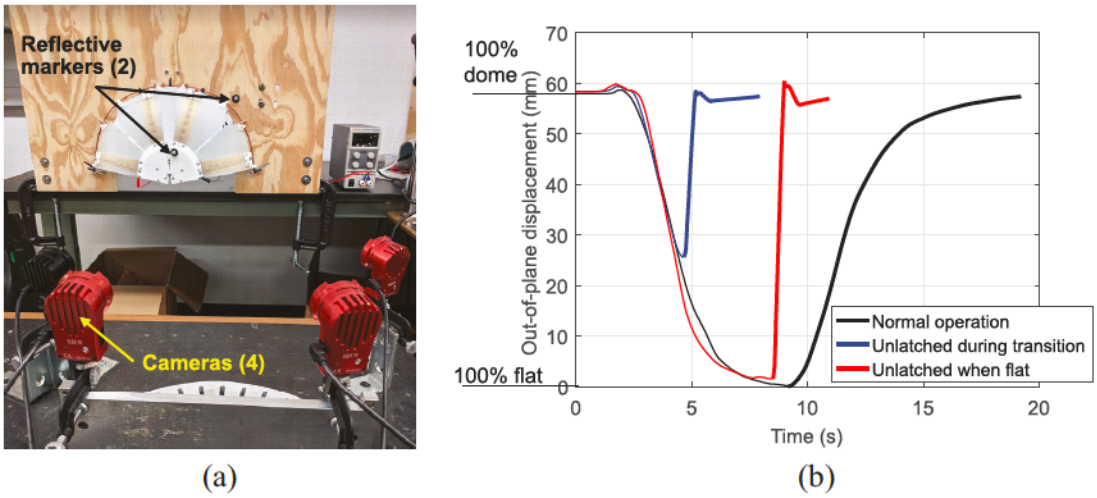

Figure 16. (a) Motion capture setup to record the morphing of a fender skirt and (b) out-of-plane displacement of the rigid segment in the fender skirt demonstrator; thin and thick lines indicate the structure's flattening and extension, respectively.

Comprehensive modeling of the fender skirt shapes requires finite-element multiphysics simulations that include kinematic constraints, fluid–structure interactions, and the thermomechanical response of SMAs.

An experimental morphing fender skirt based on smart prestressed composites has been presented and its shape transition has been demonstrated in the laboratory at half-scale. The composite structure presented is shown to have sufficient stiffness to withstand the aerodynamic loads on a cruising vehicle. For purposes of material selection, forces due to aerodynamic drag and crosswinds are assumed to act uniformly on the structure. The exact load distribution on a fender skirt can be determined using a computational fluid dynamics study and road testing on a vehicle. The results of these studies can guide decisions on the optimal domed shape for aerodynamics, the location of radial SMA actuators, and a strategy for selective actuation of the SMAs.

SMA-actuated latches are shown to be capable of quickly returning the fender skirt to the domed shape by capitalizing on the prestress in the composite ribs. An alternative to quick-release latches would be bistable composite ribs. SMA-actuated bistable composites could reduce design complexity and the overall weight of the structure. With bistable ribs, power can be turned off when the fender skirt is in the flat shape, thereby reducing actuation requirements.

To enable transition from a domed shape to a flat shape, various types of hinges are used in our demonstrator. In future versions, the hinges could be replaced with compliant joints to create a single compliant mechanism-based fender skirt. The compliant structure would have a morphing skin on its outer face, prestressed laminae on its inner face, and embedded smart-material based actuators.

Mechanically prestressed composites are attractive for combination with smart material-based actuation to achieve controllable curvature. Stretchable skins described in the literature that are suitable for morphing applications can serve as a source of prestress for creating localized curvature in a morphing surface. The passive materials used in this work are relatively inexpensive and are suitable for mass-market products such as automobiles. In conclusion, smart material-driven prestressed composites have the potential to serve as building blocks in the development of morphing vehicles that shift shape to optimize vehicle performance.

Declaration of conflicting interests

The author(s) declared no potential conflicts of interest with respect to the research, authorship, and/or publication of this article.

Funding

The author(s) disclosed receipt of the following financial support for the research, authorship, and/or publication of this article: Financial support was provided by member organizations of the Smart Vehicle Concepts Center, a National Science Foundation Industry-University Cooperative Research Center (www.SmartVehicleCenter.org). Additional support for V.S.C.C. was provided by a Smart Vehicle Center Graduate Fellowship.

Notes

1. Based on a target for fuel economy of 54.5 mpg by 2025. The estimated average fuel economy for 2015 is 41.5 mpg.
2. A 10% reduction in weight translates to a 6.5% increase in fuel economy (H-D Systems, 2013).
3. Uniaxial stretching of a thin rectangular lamina with zero in-plane Poisson's ratio results in uniform stress and strain.

ORCID iD

Venkata Siva C Chillara https://orcid.org/0000-0001-6651-3763

References

Barnard RH (1996) *Road Vehicle Aerodynamic Design: An Introduction*. Essex, England: Addison Wesley Longman Limited.

Bilgen O, Kochersberger KB, Inman DJ, et al. (2010) Novel, bidirectional, variable-camber airfoil via macro-fiber composite actuators. *Journal of Aircraft* 47(1): 303–314.

Brinson LC (1993) One-dimensional constitutive behavior of shape memory alloys: thermomechanical derivation with non-constant material functions and redefined martensite internal variable. *Journal of Intelligent Material Systems and Structures* 4(2): 229–242.

Brinson LC and Huang MS (1996) Simplifications and comparisons of shape memory alloy constitutive models. *Journal of Intelligent Material Systems and Structures* 7(1): 108–114.

Buchheim R, Leie B and Lückoff H (1983) Der neue audi 100–ein beispiel für konsequente aerodynamische personenwagen-entwicklung. *Automobiltechnische Zeitschrift* 85: 419–425.

Chapman EG, Herdic SL, Keller CA, et al. (2005) Development of miniaturized piezo-hydraulic pumps. In: *Smart structures and materials: nondestructive evaluation and health monitoring*, vol. 5762, San Diego, CA, 7–10 March, pp. 299–310. Bellingham, WA: International Society for Optics and Photonics.

Chillara VSC and Dapino MJ (2017a) Bistable morphing composites with selectively-prestressed laminae. In: *SPIE 2017 conference on smart structures and non-destructive evaluation*, vol. 10165, Portland, OR, 25–29 March. Bellingham, WA: International Society for Optics and Photonics.

Chillara VSC and Dapino MJ (2017b) Mechanically-prestressed bistable composite laminates with weakly coupled equilibrium shapes. *Composites Part B: Engineering* 111: 251–260.

Chillara VSC and Dapino MJ (2018) Stability considerations and actuation requirements in bistable laminated composites. *Composite Structures* 184: 1062–1070.

Chillara VSC, Headings LM and Dapino MJ (2016) Multifunctional composites with intrinsic pressure actuation and prestress for morphing structures. *Composite Structures* 157: 265–274.

Costelli AF (1984) Aerodynamic characteristics of the fiat UNO car. SAE technical paper 840297.

Dano ML and Hyer MW (2003) SMA-induced snap-through of unsymmetric fiber-reinforced composite laminates. *International Journal of Solids and Structures* 40(22): 5949–5972.

Daynes S and Weaver P (2010) Analysis of unsymmetric CFRP–metal hybrid laminates for use in adaptive structures. *Composites Part A: Applied Science and Manufacturing* 41(11): 1712–1718.

Deimel R and Brock O (2013) A compliant hand based on a novel pneumatic actuator. In: *2013 IEEE international conference on robotics and automation*, Karlsruhe, 6–10 May, pp. 2047–2053. New York: IEEE.

General Motors (2013) Chevrolet debuts lightweight "smart material" on corvette. *Corporate Newsroom*. Available at: http://media.gm.com/media/us/en/gm/home.detail.html/content/Pages/news/us/en/2013/Feb/0212-corvette.html

H-D Systems (2013) Future US trends in the adoption of light-duty automotive technologies. Prepared for American Petroleum Institute, September. Washington, DC: H-D Systems.

Huber JE, Fleck NA and Ashby MF (1997) The selection of mechanical actuators based on performance indices. *Proceedings of the Royal Society A: Mathematical, Physical and Engineering Sciences* 453(1965): 2185–2205.

Hucho WH (1987) *Aerodynamics of Road Vehicles: From Fluid Mechanics to Vehicle Engineering*. Oxford, UK: Butterworth-Heinemann.

Hucho WH and Ahmed SR (1998) *Aerodynamics of Road Vehicles: From Fluid Mechanics to Vehicle Engineering*. Warrendale, PA: Society of Automotive Engineers.

Hufenbach W, Gude M and Czulak A (2006) Actor-initiated snap-through of unsymmetric composites with multiple deformation states. *Journal of Materials Processing Technology* 175(1–3): 225–230.

Hyer MW (1981) Some observations on the cured shape of thin unsymmetric laminates. *Journal of Composite Materials* 15(2): 175–194.

Hyer MW (1982) The room-temperature shapes of four-layer unsymmetric cross-ply laminates. *Journal of Composite Materials* 16(4): 318–340.

Jani JM, Leary M, Subic A, et al. (2014) A review of shape memory alloy research, applications and opportunities. *Materials & Design* 56: 1078–1113.

Kim HA, Betts DN, Salo AIT, et al. (2010) Shape memory alloy-piezoelectric active structures for reversible actuation of bistable composites. *American Institute of Aeronautics and Astronautics Journal* 48(6): 1265–1268.

Koike M, Nagayoshi T and Hamamoto N (2004) Research on aerodynamic drag reduction by vortex generators. *Mitsubishi Motors Technical Review*: 11–16.

Lacasse S, Terriault P, Simoneau C, et al. (2014) Design, manufacturing, and testing of an adaptive composite panel with embedded shape memory alloy actuators. *Journal of Intelligent Material Systems and Structures* 26(15): 2055–2072.

Liang C and Rogers CA (1990) One-dimensional thermomechanical constitutive relations for shape memory materials. *Journal of Intelligent Material Systems and Structures* 1(2): 207–234.

Mattioni F, Weaver PM, Potter KD, et al. (2008) Analysis of thermally induced multistable composites. *International Journal of Solids and Structures* 45(2): 657–675.

Murray G, Gandhi F and Bakis C (2010) Flexible matrix composite skins for one-dimensional wing morphing. *Journal of Intelligent Material Systems and Structures* 21(17): 1771–1781.

Philen M, Shan Y, Wang KW, et al. (2007) Fluidic flexible matrix composites for the tailoring of variable stiffness adaptive structures. In: *48th AIAA/ASME/ASCE/AHS/ASC structures, structural dynamics, and materials conference*, Honolulu, HI, 23–26 April.

Reddy JN (1997) *Mechanics of Laminated Composite Plates: Theory and Analysis*. Boca Raton, FL: CRC Press.

Simoneau C, Terriault P, Lacasse S, et al. (2014) Adaptive composite panel with embedded SMA actuators: modeling

and validation. *Mechanics Based Design of Structures and Machines* 42(2): 174–192.
Sunny SA (2011) Effect of turbulence in modeling the reduction of local drag forces in a computational automotive model. *International Journal of Energy and Environment* 2(6): 1079–1100.
Tanaka K, Kobayashi S and Sato Y (1986) Thermomechanics of transformation pseudoelasticity and shape memory effect in alloys. *International Journal of Plasticity* 2(1): 59–72.

Appendix 1

Fender skirt dimensions

The geometry of a steered wheel relative to its fender is shown in Figure 17.

Appendix 2

Latch design

This manually-reset latch design is intended to experimentally demonstrate the rapid extension of the fender skirt. In order to quickly release the actuator SMAs, two rotary latches, one on each half of the rigid segment, are used on the demonstrator (Figure 18). Each latch is actuated using one SMA wire; the latch SMA is installed in the detwinned martensite phase. The latches are also coupled by a spring that returns them to the initial shape and the latch SMA to the detwinned martensite phase. In stages 1 and 2, the end of each actuator SMA is attached to a cantilever that is held rigidly by the latch body during normal operation. Upon heating (stage 3), the latch SMA pulls on the latch body, rotating it to disengage it from the cantilever, which bends to release tension in the actuator SMAs. To reset, the latch SMAs are turned off, the actuator SMAs are manually stretched, and the spring returns the latch body to the engaged position while stretching the latch SMA to the detwinned martensite phase.

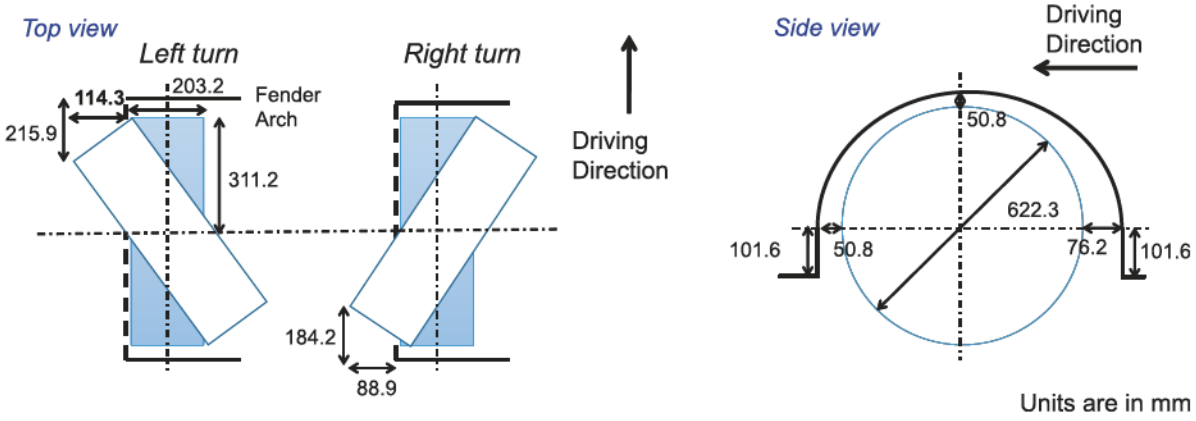

Figure 17. Approximate fender dimensions and motion limits of the left wheel of a compact passenger car.

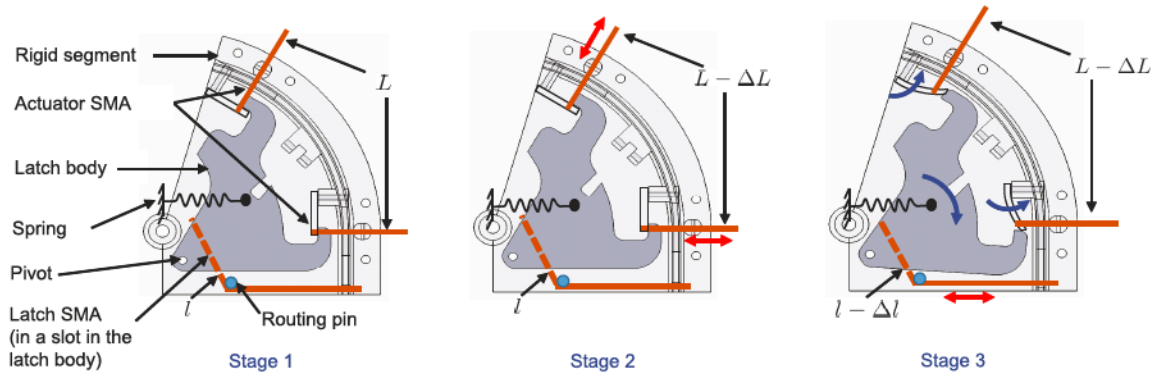

Figure 18. Latch design for the rapid release of actuator SMAs to return from an intermediate shape to the initial domed shape.